Magic compositions in Pd-Au nanoalloys

Christine Mottet, Beien Zhu, Alexis Front, Hazar Guesmi, Jérôme Creuze, Bernard Legrand

▶ **To cite this version:**

Christine Mottet, Beien Zhu, Alexis Front, Hazar Guesmi, Jérôme Creuze, et al.. Magic compositions in Pd-Au nanoalloys. Computational and Theoretical Chemistry, 2017, 1107, pp.49-56. 10.1016/j.comptc.2016.12.023 . hal-03547790

HAL Id: hal-03547790
https://hal.science/hal-03547790v1

Submitted on 31 Jan 2022

HAL is a multi-disciplinary open access archive for the deposit and dissemination of scientific research documents, whether they are published or not. The documents may come from teaching and research institutions in France or abroad, or from public or private research centers.

L'archive ouverte pluridisciplinaire **HAL**, est destinée au dépôt et à la diffusion de documents scientifiques de niveau recherche, publiés ou non, émanant des établissements d'enseignement et de recherche français ou étrangers, des laboratoires publics ou privés.

Computational and Theoretical Chemistry 1107 (2017) 49–56

Contents lists available at ScienceDirect

Computational and Theoretical Chemistry

journal homepage: www.elsevier.com/locate/comptc

Magic compositions in Pd-Au nanoalloys

Beien Zhu [a], Alexis Front [b], Hazar Guesmi [c], Jérôme Creuze [d], Bernard Legrand [e], Christine Mottet [b,*]

[a] Division of Interfacial Water and Key Laboratory of Interfacial Physics and Technology, Shanghai Institute of Applied Physics, Chinese Academy of Sciences, Shanghai 201800, China
[b] Aix Marseille Université, CNRS, CINaM UMR7325, Campus de Luminy, F13288 Marseille, France
[c] ICGM/MACS-UMR5253, 8 rue de l'Ecole Normale, F-34296 Montpellier, France
[d] Paris Sud University, Paris-Saclay University, ICMMO/SP2M, UMR8182, 15 rue Georges Clmenceau, F-91405 Orsay, France
[e] SRMP-DMN, CEA Saclay, Paris-Saclay University, F-91191 Gif-sur-Yvette, France

ARTICLE INFO

Article history:
Received 17 October 2016
Received in revised form 6 December 2016
Accepted 13 December 2016
Available online 18 December 2016

Keywords:
Monte Carlo simulations
Metallic alloy nanoparticles
Surface segregation
Chemical ordering

ABSTRACT

We identified new magic compositions of Pd-Au nanolloys of simple symmetries according to the icosahedral and the cubic truncated octahedral structures. Chemically ordered structures as well as segregated ones are characterized using Monte Carlo simulations in semi-grand canonical ensemble and tight-binding semi-empirical potential fitted to *ab initio* calculations for the Pd-Au system. Ordering and surface (or core) segregation phenomena can be distinguished by their behavior as a function of the temperature: chemical ordering at surface or in the core disappears above a critical temperature (which is lower or equal to the bulk alloy order-disorder temperature), whereas surface/core segregation (core-shell structures) remains at high temperature, although the interfacial profile is less abrupt.

© 2016 Elsevier B.V. All rights reserved.

1. Introduction

Nanoalloys are commonly nanoparticles of alloys where both size and composition influence their structures and properties. They represent a very attractive and intensive domain of research from the last tens years [1–3], notably because they present exciting chemical and physical (magnetism, plasmonic) properties with applications in numerous domains as catalytic reactions, fuel cells, cancer detection and treatment, ... The control of the size, structure and composition is a crucial point in order to master the properties and applications. In case of nanoalloys, not only the size and composition but also the chemical ordering associated to the atomic structure, morphology and temperature must be controlled in order to properly characterize the nanoalloy structure, giving rise to nanoalloys phase diagram.

There are two kinds of theoretical approach to study nanoalloys phase diagrams. On one side, the global optimization methods as genetic algorithm [4–6] or basin-hopping procedure [7–9] are methods of choice to search for the lowest energy structure of nanoclusters and nanoalloys inside a complex energy landscape involving a global search either on the atomic structure (without any symmetry restriction) and the chemical configuration. However these methods are limited to relatively small sizes and are concentrated on the fundamental state at zero Kelvin (no temperature). Nonetheless, such global optimization methods are very efficient to discover new original symmetries (far from the bulk metal cubic symmetry) and chemical ordering adopted by small nanoalloys of less than one hundred of atoms [10]. Moreover, it gives not only the lowest energy minimum but also a series of higher energy isomers allowing to reconstruct the partition function in the harmonic approximation and get some thermodynamics of the systems [11–13]. On the other side, and rather when we are interested in larger cluster sizes (some hundreds to thousands of atoms), the symmetry of the systems can be restrained to a few different motifs (icosahedron, decahedron and truncated octahedron) for which it is sufficient to perform global optimization only on the chemical configuration with possible local atomic relaxations. The methods consist of Metropolis Monte Carlo simulations with chemical exchange and eventually atomic displacements. They give rise to a statistical and therefore thermodynamical study of the systems either on lattice-model Hamiltonian with effective interactions derived from Tight-Binding Ising model [14–16] or Cluster Expansion Method [17], or within local atomic relaxations using semi-empirical potentials [18–20].

For specific systems, with a chemical demixing tendency (typically core-shell nanoalloys), the global optimization method has been extended to quite large systems (some hundreds of atoms) by performing tailored chemical exchanges according to their local environment instead of random exchanges as in Metropolis Monte Carlo [21–23]. Such tailored global optimization algorithm increases the efficiency of the search of the lowest energy structure

* Corresponding author.
E-mail address: mottet@cinam.univ-mrs.fr (C. Mottet).

http://dx.doi.org/10.1016/j.comptc.2016.12.023
2210-271X/© 2016 Elsevier B.V. All rights reserved.

in demixing nanoalloys [22,23] allowing to compare theoretical results with experiments performed by high resolution transmission electron microscopy on the Cu-Ag system whith core-shell and Janus structures [24].

Such improvement is not efficient in case of alloys with ordering tendency so that to study the equilibrium structures of Pd-Au nanoalloys on a quite large range of size we use Metropolis Monte Carlo simulations and local atomic relaxations on starting symmetries according to simple motifs like icosahedra, decahedra or truncated octahedra. In a previous study we have characterized the stability domain of each motif finding that the range of size where the icosahedral structure is stable over the decahedral and truncated octahedral structure is greatly enhanced in bimetallic nanoparticles as compared to each of the pure ones [20]. The raison comes from the strain relaxation in the core of the icosahedron which is compressed in pure systems whereas in case of lattice misfit between the two elements, the smaller one goes into the core to release the strain and reduces the excess energy of the icosahedron core whereas the energy gain of the icosahedral structure comes from its dense and spherical surface (only (1 1 1) facets).

Pd-Au nanoalloys have promising properties in catalytic processes [25–28] and electrocatalysis [29]. To understand and control the reaction it is necessary to know the chemical nature and ordering on the surface of the catalyst, which is experimentally not trivial. This is why numerical simulation of the structure and chemical ordering is required in order to investigate the raison of the good catalytic activity and or selectivity.

In the present study we will show how magic compositions can be revealed by Monte Carlo simulation in semi-grand canonical ensemble on different nanoalloys structures and sizes. These magic compositions are all the more significant than the cluster size is small. We also notice different occupation rules of the different species as a function of the type of sites as compared to larger sizes. Finnally we will characterize the segregation effects from the ordering ones depending on the existence of a transition of the type order/disorder or demixion/disorder as a function of temperature.

The paper is organized in four sections including Introduction and Conclusion parts. The second section details the energetic model and simulation method. The third section is devoted to the results on two different motifs: icosahedron (Section 3.1), truncated octahedron (Section 3.2) and transitions with temperature (Section 3.3).

2. Theoretical method

The theoretical method is based on Metropolis Monte Carlo simulations in semi-grand canonical ensemble where the interatomic energy comes from a semi-empirical tight binding model in the second moment approximation of the density of states (TBSMA). Such method has been described in a previous study [20] together with the interatomic potential for Pd-Au alloys.

We just recall that the potential energy at site i for an atom of type a is written as follows:

$$E_i^a = -\sqrt{\sum_{j,r_{ij}<r_{ab}^c} \xi_{ab}^2 e^{-2q_{ab}\left(\frac{r_{ij}}{r_{ab}^0}-1\right)}} + \sum_{j,r_{ij}<r_{ab}^c} A_{ab} e^{-p_{ab}\left(\frac{r_{ij}}{r_{ab}^0}-1\right)} \quad (1)$$

where r_{ij} is the distance between the atom at site i and their neighbors at site j, r_{ab}^c is the cut-off distance and r_{ab}^0 is the first neighbor distance depending on the nature of the atoms, and $p_{ab}, q_{ab}, A_{ab}, \xi_{ab}$ are four parameters (listed in Table 1). These parameters have been fitted to the values of the cohesive energies, lattice parameters and elastic constants for the pure metals, and to the mixing energies in the diluted limits calculated using the density functional theory (DFT) with the local-density approximation (LDA) for the exchange and correlation functional [20].

We notice in Table 1 that the difference in cohesive energy of the two metals as given by the DFT-LDA calculations is higher than the experimental one (−3.94 eV/at. and −3.81 eV/at. respectively for Pd and Au from Kittel [30]). In fact neither the LDA nor the GGA exchange and correlation functional give satisfying results for both metals. In Ref. [20] we give all the values of lattice parameters, cohesive energies and surface energies of Au and Pd and made the choice of the LDA to fit the TBSMA potential. Fitting the potential to *ab initio* calculations instead of experimental values allows to fit the mixed interactions to quantities as the permutation energies which does not exist experimentally.

We use Monte Carlo simulations with the Metropolis algorithm in the semi-grand canonical ensemble where the temperature, pressure and number of atoms are fixed but the composition (number of atoms of Pd and Au) varies as a function of the difference of the chemical potential between the two elements ($\Delta\mu = \mu_{Au} - \mu_{Pd}$). The different Monte Carlo trials comprise atomic displacements and chemical permutations on atomic sites. Each macrostep of the Monte Carlo simulation consists to select randomly a displacement procedure or a chemical permutation procedure and then to select randomly one atom on which we propose a displacement (or a chemical permutation, depending on the procedure) and to repeat this trial as much as times that there are atoms in the system. Usually we perform ten times more displacements than chemical permutations in order to let the system relax according to different chemical configurations. Typically using ten thousands of macrosteps, we perform in total some tens millions of trials, using half of them to reach the equilibrium, the other half to perform statistical averages.

3. Results

We considered two different structures among the typical high symmetry structures (icosahedron, decahedron and truncated octahedron) which represent the equilibrium structure on a large range of size [20]. The icosahedral structure is a typical fivefold symmetry structure whose morphology is the most spherical one and contains only (1 1 1) facets, as compared to truncated octahedral or decadrehal one. The price to pay is to strain atomic distances in the core as compared to the bulk structure. We compared the icosahedral structures and chemical arrangements at low temperature (fundamental state) with fivefold symmetry to the ones within the truncated octahedral structure (bulk face centered cubic symmetry). The high-symmetry structures are taken as initial atomic configurations but the Monte Carlo simulations that we perform allow symmetry-unrestricted optimization which means the final stable structure can break the initial symmetry, except the magic atoms number, corresponding to full compact atomic structure with the original symmetry. Finally we analyze the chemical transitions as a function of temperature.

3.1. Magic compositions on icosahedral Pd-Au nanoalloys

We studied the icosahedra (Ih) of 55, 147 and 309 atoms (less or equal to 2 nm) and compare their chemical arrangement to what has been obtained on large clusters (6525 atoms, around 6 nm of diameter) [20] to analyze possible size effects in the chemical ordering and surface segregation.

Using Monte Carlo simulations we calculate the equilibrium composition as a function of the difference in chemical potential ($\Delta\mu$) at low temperature (isotherms at 80 K). For the smaller size

Table 1
Parameters of the Pd-Au TBSMA potential.

$a-b$	E_{coh} (eV)	a (Å)	p_{ab}	q_{ab}	A_{ab}	ξ_{ab}
Pd-Pd	−4.98	3.85	11.75280	2.87486	0.14352	1.88570
Au-Au	−4.24	4.08	10.71890	4.09805	0.22043	1.97573
Pd-Au			11.23585	3.48645	0.21410	2.08060

(55 atoms) magic compositions are very well characterized. Indeed, we notice on the upper graph of the Fig. 1 that the curve presents different steps corresponding to particularly stable chemical configurations. Each step is associated to the filling by gold atoms of certain types of site (see Fig. 1 lower graph): first the verteces are occupied by gold atoms, which corresponds to the cluster $Pd_{43}Au_{12}$, then the edges started to be filled. Whereas the curve representing the concentration of gold atoms on the edges is a straight line, we observe two small steps of the chemical potential curve. So we plotted the edge concentration as a function of the chemical potential (Fig. 2). We see clearly two steps corresponding to the composition of 1/3 and 2/3 of the total edge sites. We must keep in mind that the 55-atom Ih has just vertex and edge sites at its surface, which gives also triangular facets of the (1 1 1) type but these sites are properly vertex and edge sites. For a composition of 1/3 gold atoms on edge sites, we obtain the structure of the Fig. 1(b) whith a countinuous atomic chain of gold atoms which runs all around the surface, intermixed with a continuous atomic chain of Pd atoms. This is a quite low symmetry structure but with a particular stable chemical ordering. Only one edge over three is occupied by gold atoms. The next stable configuration with 2/3 of edge sites occupied by gold atoms consists of a more symmetric structure with one Pd atom remaining on each "triangular facet" (Fig. 1(c)), which are in fact made of edge and vertex sites. Finally, the next magic composition corresponds to the well known core-shell structure which has been characterized rather in systems with demixion tendency [31]. The fact that we observe it in the miscible Pd-Au system results from the gold surface segregation tendency which comes from the difference in surface energy (or cohesion energy) between Au and Pd and also because Au atoms are larger than Pd atoms. Even if we overestimate the difference in cohesive energy between the two metals, we can guess

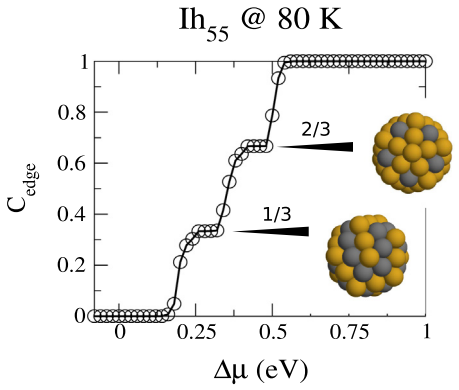

Fig. 2. Edge concentration as a function of the chemical potential difference. The magic concentrations $Pd_{33}Au_{22}$ and $Pd_{23}Au_{32}$ correspond to respectively 1/3 and 2/3 gold atoms over the all edge sites.

that this result would remain because of the difference in surface energy and the difference of size of the two metals.

The next magic number is the 147-atom icosahedron with one atom on each (1 1 1) facet. We can again notice some magic compositions on the curve representing the chemical potential as a function of the global composition in the cluster. The first stable composition is the one with all the verteces occupied by gold atoms ($Pd_{135}Au_{12}$). Then, instead of populating the edge sites according to the increasing of the coordination number as we observe on large clusters [20], the (1 1 1) facet sites are populated by gold atoms (Fig. 3(b)) before the edges. Such inversion of the surface segregation which usually follows the progression from low coodinated sites to higher coordinated sites (vertex, edge,

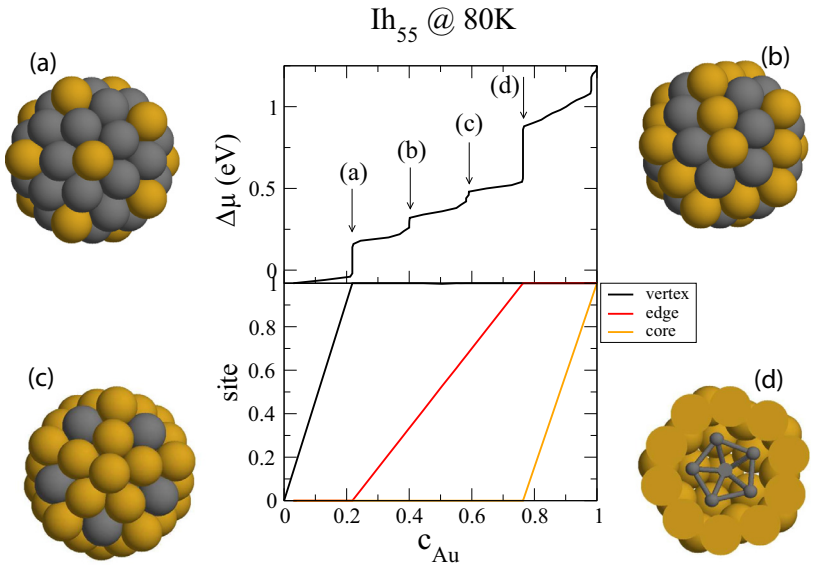

Fig. 1. Isotherm at 80 K of a 55-atom icosahedron: first row, the chemical potential difference ($\Delta\mu = \mu_{Pd} - \mu_{Au}$) as a function of the Au composition "c_{Au}" and second row, the composition on each type of site (vertex, edge and core) as a function of the global concentration "c_{Au}". Magic concentrations are characterized: (a) $Pd_{43}Au_{12}$, (b) $Pd_{33}Au_{22}$, (c) $Pd_{23}Au_{32}$, (d) $Pd_{13}Au_{42}$.

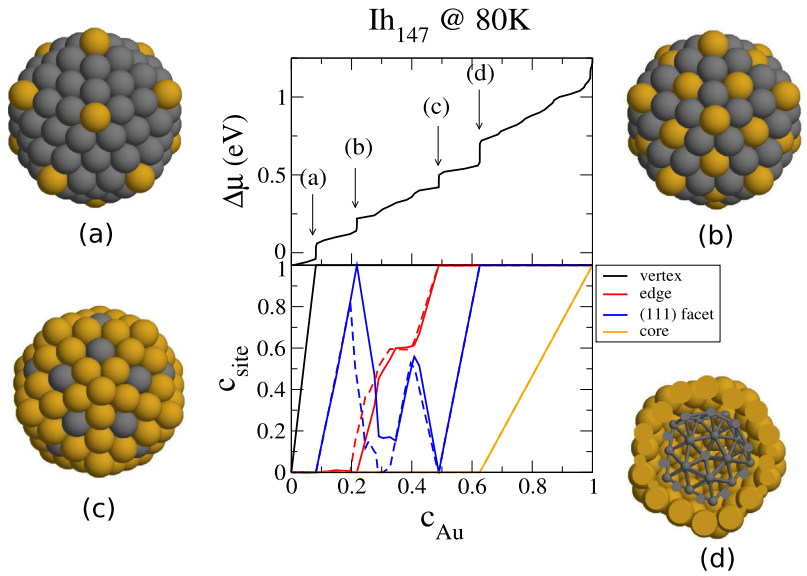

Fig. 3. The same as Fig. 1 for 147-atom icosahedron with magic concentrations: (a) $Pd_{135}Au_{12}$, (b) $Pd_{115}Au_{32}$, (c) $Pd_{75}Au_{72}$, (d) $Pd_{55}Au_{92}$. The dashed lines represent the simulations where $\Delta\mu$ is decreasing whereas continuous lines represent the simulations where $\Delta\mu$ is increasing. Usually the curves are superimposed.

(100) facets and (111) facets) has already been noticed due to finite-size effects in Cu-Ag truncated octahedra between (100) and (111) facets [32,15]. It has been explained by an indirect coupling between facets and edges. We observe a similar behavior here where the gold occupation on edges and facets (see Fig. 3) are in competition giving rise to the structures (b) and (c). In the structure (b) ($Pd_{115}Au_{32}$), the facets are occupied by one gold atom (which is sufficient to fill the facets) and the edges remain pure in Pd whereas it is the opposite in the structure (c) ($Pd_{75}Au_{72}$) where the facets are occupied by one Pd atom (no gold) and the edges are pure in Au. From a simple point of view of the total number of sites on edges and facets, as there are three times more edge sites (60) than facet sites (20) (which is unusual), it is more convenient to fill the (111) facets first, letting the edges be filled by Pd atoms to form the motif of the $(\sqrt{3}\times\sqrt{3})$ R30 of the (111) PdAu reconstructed surface, on Pd-rich side, and then the opposite, whith a Pd atom on each (111) facet surrounded by Au pure edges, on Au-rich side. The transition between the structures (b) and (c) is not well defined as shown by the curves of edge and facet concentration in Fig. 3 where we can notice that when we vary $\Delta\mu$ by increasing (continuous line) or decreasing (dashed line) values of $\Delta\mu$, the curves are not superimposed. Finally, the next magic composition corresponds to the core-shell structure with a core of 55 Pd atoms and a monoatomic surface layer of gold.

By increasing the cluster size with one more atomic layer on the former structure leading to the 309-atom Ih, we would like to see if we start to converge toward a general segregation/ordering profile with more or less no size effect. In the Fig. 4, we recognize the behavior of large size icosahedra (Ih_{6525} [20]) with the filling of the different surface sites according to their coordination number: first the verteces, then the edges with a plateau corresponding to an ordering between the Pd and Au atoms along the edges (without frustrations with the verteces), then the (111) facets and finally the core. Edge and facet sites segregation curves are noisy (up and down curves are not superimposed) probably due to complexe interactions and chemical frustrations from structure (b) to (c). The alternance of Au and Pd atoms along the edges have been observed for the large cluster [20]. The edge ordering interacts obviously with the verteces leading to an ordering frustration if the number of sites along the edges is pair because the verteces are initially occupied by gold atoms. In the case of 309-atom Ih, the edges consist of three atoms so preventing any frustration. This is rather the coupling between the facet sites (3 atoms) and the edge sites (3 atoms) which leads to some noise in the curves but we can distinguish a small step in the facet concentration at 0.66 which corresponds to two Au atoms for one Pd, even if it does not appear clearly on the curve of the chemical potential. The next noticable structure is the core-shell (Fig. 4(c)) with a small step on the chemical potential and which corresponds to the completion of the surface layer whereas the core remains pure in Pd. The core-shell interface is really abrupt as compared to the large size (Ih_{6525} [20]) where the core begins to be filled whereas the surface is not fully Au-pure. The last noticable structure is less known than the core-shell structure, but it has been already described in larger icosahedra [20]. It presents a small Pd cluster in the center of the core, where the local compression is the higher, and other Pd atoms are dispersed in the core with a local chemical ordering leading to optimize the mixed bonds, except along radial directions where Pd atoms are aligned as can be see on the Fig. 4(d). Such structure is typical of the ability of the icosahedral nanoalloys to accommodate the internal stress by putting smaller atoms in the center of the core [31,20] and exists for any size as shown on the Fig. 4 for the 561, 923 and 6525 atoms icosahedra.

3.2. Magic compositions on truncated octahedral Pd-Au nanoalloys

We considered three sizes of truncated octahedron (TOh) with 38, 201 and 405 atoms. The 38-atom TOh is a particular stable structure keeping the face centered cubic (fcc) symmetry whereas icosahedral or polyicosahedral structures are usually the most stable at small sizes. The energy landscape of the 38-atom Lennard-Jones pure cluster presents two funnels [33]: a deep and narrow one corresponding to the fcc TOh structure global minimum and a much wider and slightly higher in energy corresponding to an incomplete icosahedron. Moreover there is a large energy barrier between the two funnels which makes it difficult to go from one to the other. For binary Lennard-Jones clusters where the atomic size differs from the two constituents, the global optimization search does not find the 38-atom structure as a global minimum. Indeed when only the size mismatch is concerned (and eventually a chemical demixion tendency [31] leading to a core-

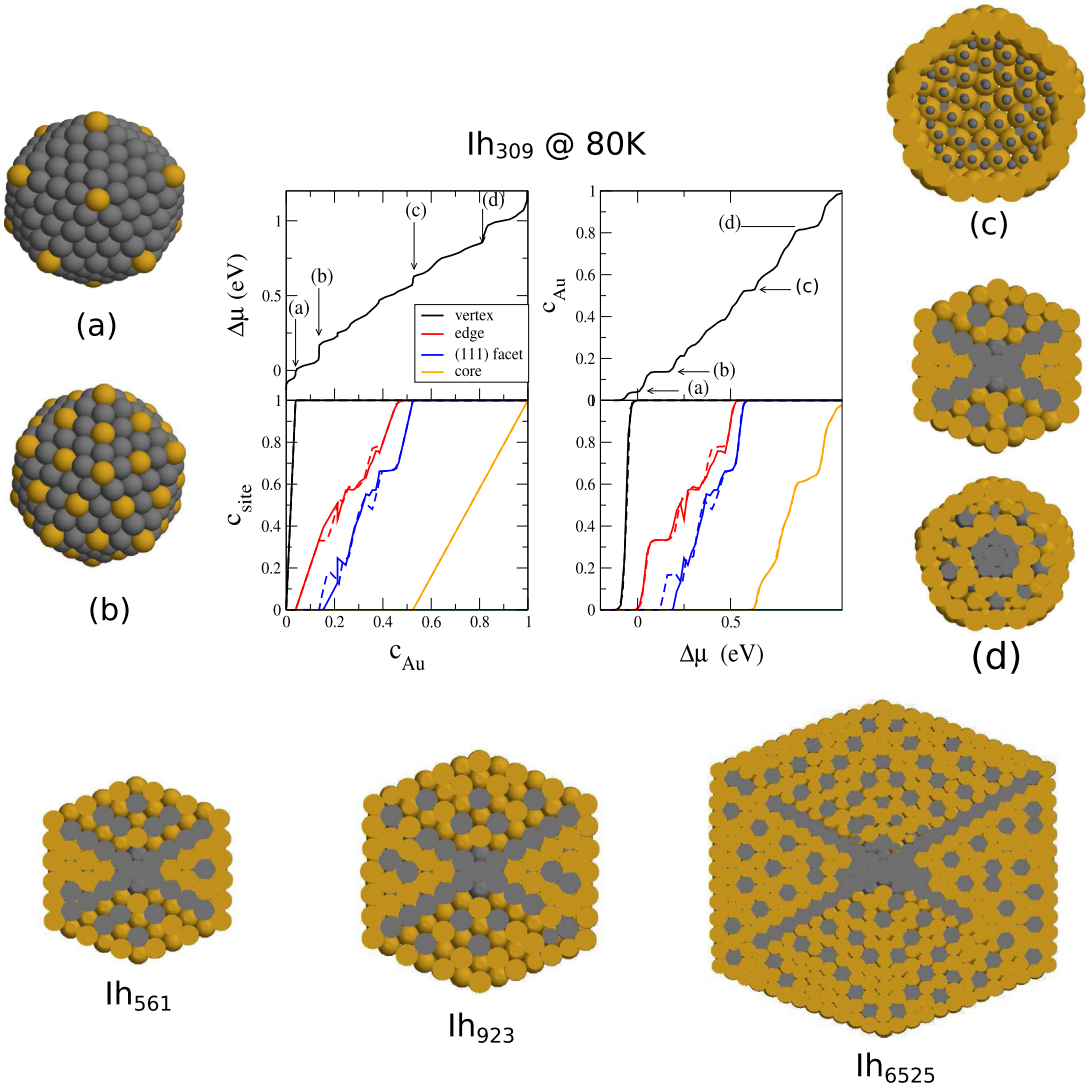

Fig. 4. 309-atom icosahedron with magic concentrations: (a) $Pd_{297}Au_{12}$, (b) $Pd_{267}Au_{42}$, (c) $Pd_{147}Au_{162}$, (d) $Pd_{57}Au_{252}$. The first row represents the chemical potential difference ($\Delta\mu$) as a function of the gold concentration (on the left) and vice versa (on the right). The second row represents the gold concentration on each type of site as a function of the global gold concentration and as a function of $\Delta\mu$. Continuous line for simulations with increasing (up) $\Delta\mu$ and dashed lines for decreasing (down) $\Delta\mu$.

shell structure), the 34-atom and 45-atom polyicosahedral structures are prefered [10].

In the Pd-Au system, the chemical mixing tendency favors Au-Pd mixed bonds at the surface and in the core, which does not lead to the core-shell structure. A global optimization as a function of the composition has been performed for the 34-atom and 38-atom Pd-Au clusters [34] using three different parameterizations of the TBSMA potential (Gupta many-body empirical potential). In particular, the composition $Pd_{14}Au_{24}$, which is one of the magic compositions we found for the 38-atom TOh (Fig. 5(b)) with all the verteces occupied by Au atoms and the (1 1 1) facet and core occupied by Pd, corresponds to the lower mixing enthalpy in the all range of concentration within the DFT-fit. This is a nice check of the validity of our new potential also fitted to DFT calculations, and of the relevance of our method. The 38-atom TOh cluster presents two other clear magic compositions: the one with half of the vertex atoms occupied by Au ($Pd_{26}Au_{12}$) and the perfect core-shell structure (Pd_6Au_{32}).

The next TOh structure with complete atomic shell is the 201-atom size where there are one site on each (1 0 0) facet and a complete hexagon (seven sites) on each (1 1 1) facet. We still distinguish clearly magic compositions on the Fig. 6. The first one

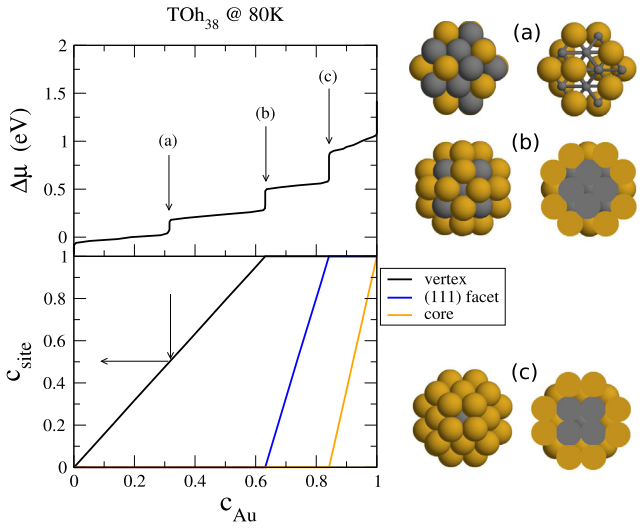

Fig. 5. Chemical potential difference ($\Delta\mu$) and site concentration as a function of the global Au concentration (c_{Au}) for 38-atom truncated octahedron with magic concentrations: (a) $Pd_{26}Au_{12}$, (b) $Pd_{14}Au_{24}$, (c) Pd_6Au_{32}.

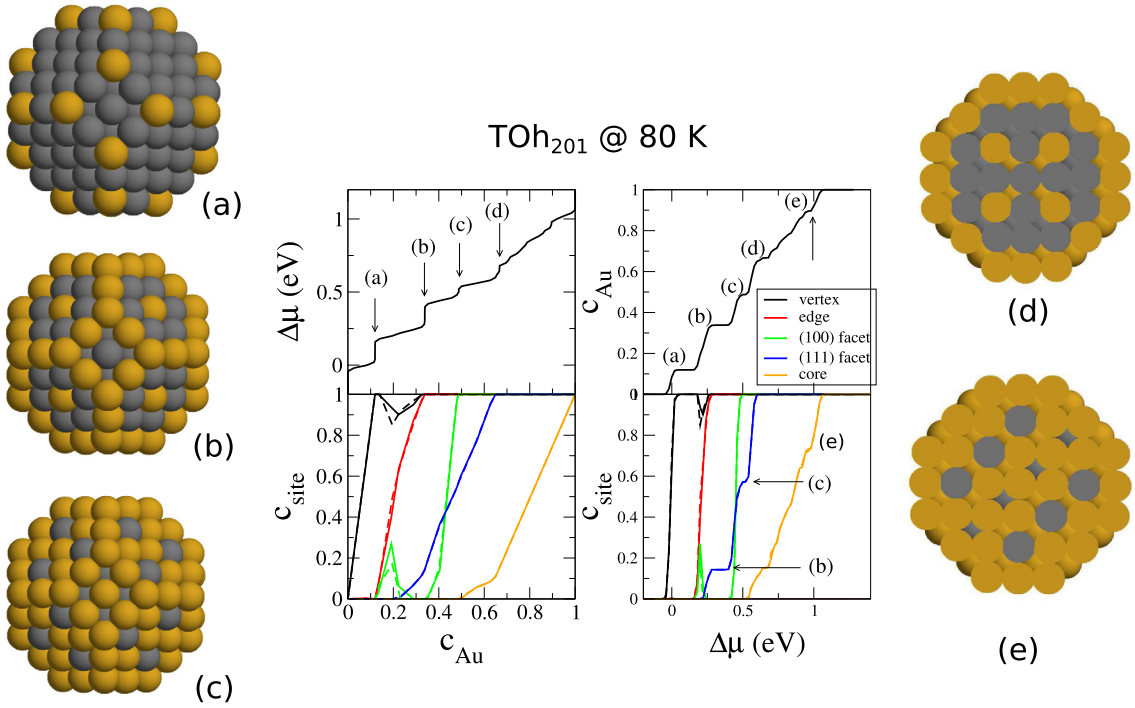

Fig. 6. 201-atom truncated octahedron with magic concentrations: (a) $Pd_{177}Au_{24}$, (b) $Pd_{133}Au_{68}$, (c) $Pd_{103}Au_{98}$, (d) $Pd_{67}Au_{134}$ and (e) $Pd_{22}Au_{179}$. The first row represents the chemical potential difference ($\Delta\mu$) as a function of the gold concentration (on the left) and vice versa (on the right). The second row represents the gold concentration on each type of site as a function of the global gold concentration and as a function of $\Delta\mu$. Continuous line for simulations with increasing (up) $\Delta\mu$ and dashed lines for decreasing (down) $\Delta\mu$.

corresponds to all the verteces filled by Au ((a) $Pd_{177}Au_{24}$). Before the next magic composition, there are some interactions between the verteces, the edges and the (100) sites, leading to a non linear evolution of the concentration on edge sites. Even if all the edges are composed of only one single site, so that there is no chemical frustration on one edge, all the edges are not filled independently from the others and there is some interaction between the edge sites and the (100) facet sites. Some of the (100) sites are filled before the (111) facets. Finally all the edges and the center of the (111) are filled with Au ((b) $Pd_{133}Au_{68}$). In the next noticable composition, all the (100) facets are pure in gold while the (111) present the $(\sqrt{3}\times\sqrt{3})$ R30 superstructure ((c) $Pd_{103}Au_{98}$). These two specific chemical ordering on the (111) facets correspond to the steps on the site concentration of the (111) facets as a function of $\Delta\mu$. After that, there is no perfect core-shell structure since the core is slightly filled with a certain ordering in the inner core, while the sub-surface layer is pure in Pd ((d) $Pd_{67}Au_{134}$). The last structure ((e) $Pd_{22}Au_{179}$) is finally ordered according to the DO_{22} $PdAu_3$ bulk ordered phase in the core with a pure gold surface. This is already what we get in larger TOh clusters [20].

For the next higher size of TOh, the 405-atom TOh depicted on Fig. 7, we still notice a quite important interaction between the vertex, edge and (100) facet concentration. We also have the tendency to fill the (100) facet before the (111) but there again with a strong interaction at low concentration as can be seen on the structure (c) $Pd_{297}Au_{108}$ where the (100) and (111) facets are partially filled. But as soon as the (100) facets are Au-pure, the (111) facets display the $(\sqrt{3}\times\sqrt{3})$ R30 superstructure in the structure (d) $Pd_{245}Au_{160}$. As the 201-atom TOh, the 405-atom one does not present a core-shell structure because as soon as the surface is Au-pure the core is already mixed with a certain ordering as for the 201-atom TOh but not as the 8678-atom TOh studied in Ref. [20] where the core ordering was similar to the one in bulk phase diagram (the A_2B_2-type). In the present case we rather get onion-shell structure near the surface, extending to the sub-surface and sub-sub-surface. Then the inner core looks like an ordered phase. The last remarkable composition also seems ordered as for a $PdAu_3$ phase in the inner core (rather $L1_2$) with antiphase bounding in the sub-surface compatible with a DO_{22} ordering. So there are still some finite size effects relative to the matching of the gold surface segregation with the core chemical ordering.

3.3. Temperature effect on the chemical arrangement

From the previous results we have seen that the chemical arrangement comes from two different phenomena: the surface segregation of gold and the chemical ordering at the surface and in the core. The temperature has different effects on these two phenomena. The surface segregation is slightly attenuated with increasing temperature according to the well known equilibrium equation in mean-field approximation [32,35]:

$$\frac{c_p}{1-c_p} = exp\left(-\frac{\Delta H_p - \Delta\mu}{k_B T}\right) \tag{2}$$

which means that when the temperature increases, c_p decreases but as can be seen on the curves of Fig. 8, the segregation remains up to high temperature (500 K). In absence of segregation, all the site concentration would be on the first diagonal of the graphs on the right column of Fig. 8.

Concerning the chemical ordering, we notice on the left column of Fig. 8 that the steps at low temperature desappear at high temperature, at least around 300 K, which correspond to the order-disorder transition critical temperature of our bulk system. This means that the 55-atom icosahedron with the magic compositions: $Pd_{33}Au_{22}$ and $Pd_{23}Au_{32}$ where we get this "snake" structure and the other chemical arrangement with one Pd atom surrounded by gold atoms, are not stable by increasing the temperature. This is the

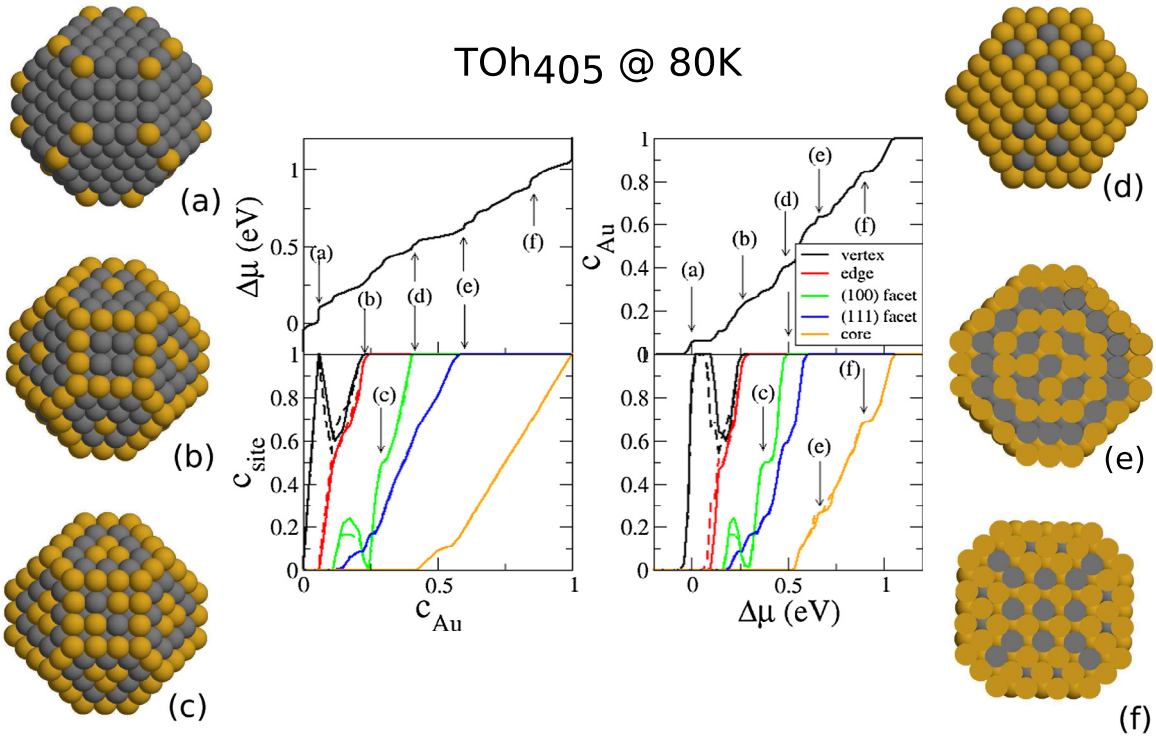

Fig. 7. The same as Fig. 6 for 405-atom TOh with magic concentrations: (a) $Pd_{381}Au_{24}$, (b) $Pd_{325}Au_{80}$, (c) $Pd_{297}Au_{108}$, (d) $Pd_{245}Au_{160}$, (e) $Pd_{147}Au_{258}$ and (f) $Pd_{63}Au_{342}$.

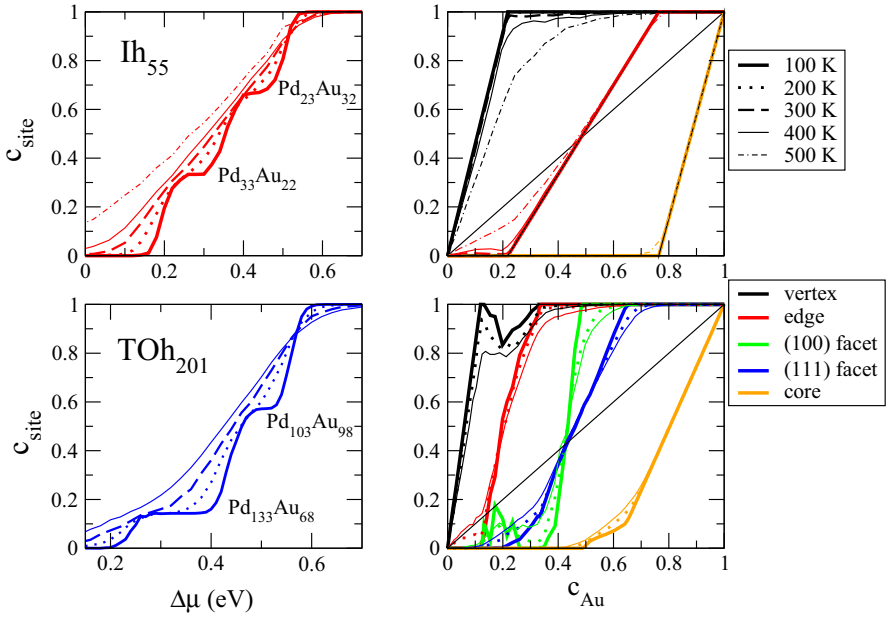

Fig. 8. Concentration isotherms as a function of the chemical potential difference on the left column and as a function of global concentration on the right colum for the 55-atom Ih and the 201-atom TOh at different temperatures (100 K with thick continuous line, 200 K with dotted line, 300 K with dashed line, 400 K with thin continuous line and 500 K with thin dashed-dotted line). The types of site are represented with the same color code as in the preceding figures.

same behavior for the chemical ordering on the (1 1 1) facets of the TOh_{201} following the motif of the $(\sqrt{3} \times \sqrt{3})$ R30 superstructure of the infinite (1 1 1) surface.

It has to be noticed here that the bulk critical order-disorder transition temperature of our model Pd-Au alloy (around 300 K) is probably underestimated as compared to the experimental one (this one being not well known [36]) we just has to recall that the temperature of our model could be rescalled in order to fit the experimental one.

3.4. Conclusions

We have characterized in this paper the magic compositions of Pd-Au nanoalloys of high symmetry (Ih and TOh) for which chemical ordering tendency can be in competition with segregation ten-

dency. In systems with the demixion tendency, the segregation effects are cooperative with phase separation leading to core-shell or Janus structures [23]. We have seen that in the Pd-Au system, the gold surface segregation can be antagonist with the chemical ordering (making mixed Pd-Au bonds) leading to chemical frustrations. However, there are also well ordered and particularly stable structures which can accommodate the two tendencies as core-shell structures for given magic compositions espacially in icosahedral structures but also chemically ordered mixed surfaces with pure Pd core (in icosahedra) or pure Au surface shell with chemically ordered core in truncated octahedra. In general, the surface sites are populated from the lower coordinated sites up to the higher ones but the chemical ordering can induce interactions between the composition of each type of sites. The (1 1 1) facets have the tendency to reproduce the $(\sqrt{3} \times \sqrt{3})$ R30 superstructure of the infinite (1 1 1) Pd-Au surface.

The semi-grand canonical Monte Carlo simulation is a method of choice to characterize magic composition of nanoalloys and to study the order-disorder transition as a function of the temperature.

Finally we have shown some specific chemical arrangements as a function of cluster size, essentially for small sizes, as compared to the general ones at larger sizes [20].

Acknowledgements

We acknowledge support from the French Research National Agency under the Project ANR-11-JS07-0007 and the French HCP ressources: CCRT/CINES/IDRIS under the allocations 2012 [x2012086395] and 2013-096829.

References

[1] Roy L. Johnston, Riccardo Ferrando, Nanoalloys: from theory to application, Faraday Discuss. 138 (2008).
[2] R. Ferrando, J. Jellinek, R. Johnston, Nanoalloys: from theory to applications of alloy clusters and nanoparticles, Chem. Rev. 108 (2008) 845.
[3] R. Ferrando, R.L. Johnston, C. Louis, PCCP themed issue: recent advances in the chemical physics of nanoalloys, PHys. Chem. Chem. Phys. 17 (2015) 27903.
[4] S. Darby, T.V. Mortimer-Jones, Roy L. Johnston, C. Roberts, Theoretical study of Cu-Au nanoalloy clusters using a genetic algorithm, J. Chem. Phys. 116 (2002) 1536.
[5] A. Rapallo, G. Rossi, R. Ferrando, A. Fortunelli, B.C. Curley, L.D. Lloyd, G.M. Tarbuck, R.L. Johnston, Global optimization of bimetallic cluster structures. I. Size-mismatched Ag-Cu, Ag-Ni, and Au-Cu systems, J. Chem. Phys. 122 (2005) 194308.
[6] G. Rossi, R. Ferrando, A. Rapallo, A. Fortunelli, B.C. Curley, L.D. Lloyd, R.L. Johnston, Global optimization of bimetallic cluster structures. II. Size-matched Ag-Pd, Ag-Au, and Pd-Pt systems, J. Chem. Phys. 122 (2005) 194309.
[7] D.J. Wales, J.P.K. Doye, Global optimization by basin-hopping and the lowest energy structures of Lennard-Jones clusters containing up to 110 atoms, J. Phys. Chem. A101 (1997) 5111.
[8] R. Ferrando, A. Fortunelli, R.L. Johnston, Searching for the optimum structures of alloy nanoclusters, Phys. Chem. Chem. Phys. 10 (2008) 640.
[9] G. Rossi, R. Ferrando, Searching for the low-energy structures of nanoparticles: a comparison of different methods and algorithms, J. Phys.: Condens. Matter 21 (2009) 084208.
[10] J.P.K. Doye, L. Meyer, Mapping the magic numbers in binary Lennard-Jones clusters, Phys. Rev. Lett. 95 (2005) 063401.
[11] J.P.K. Doye, F. Calvo, Entropic effects on the size dependence of cluster structure, Phys. Rev. Lett. 86 (2001) 3570.
[12] F. Calvo, J.P.K. Doye, D.J. Wales, Equilibrium properties of clusters in the harmonic superposition approximation, Chem. Phys. Lett. 366 (2002) 176.
[13] E. Panizon, R. Ferrando, Solid-solid transitions in Pd-Pt nanoalloys, Phys. Rev. B 92 (2015) 205417.
[14] B. Yang, M. Asta, O.N. Mryasov, T.J. Klemmer, R.W. Chantrell, The nature of A1-L10 ordering transitions in alloy nanoparticles: A Monte Carlo study, Acta Mater. 54 (16) (2006) 4201–4211.
[15] F. Lequien, J. Creuze, F. Berthier, I. Braems, B. Legrand, Superficial segregation, wetting, and dynamical equilibrium in bimetallic clusters: A Monte Carlo study, Phys. Rev. B 78 (2008) 075414.
[16] A. Lopes, G. Treglia, C. Mottet, B. Legrand, Ordering and surface segregation in CoPt nanoparticles: a theoretical study from surface alloys to nanoalloys, Phys. Rev. B 91 (2015) 035407.
[17] R.V. Chepulskii, W.H. Butler, Tuning of L10 atomic order in Co-Pt nanoparticles: Ab initio insights, Phys. Rev. B 86 (2012) 155401.
[18] L. Delfour, J. Creuze, B. Legrand, Exotic behavior of the outer shell of bimetallic nanoalloys, Phys. Rev. Lett. 103 (2009) 205701.
[19] Y. Wang, M. Hou, Ordering of bimetallic nanoalloys predicted from bulk alloy phase diagrams, J. Phys. Chem. C 116 (2012) 10814.
[20] B. Zhu, H. Guesmi, J. Creuze, B. Legrand, C. Mottet, Crossover among structural motifs in PdAu nanoalloys, Phys. Chem. Chem. Phys. 17 (2015) 28129.
[21] D. Bochicchio, R. Ferrando, Size-dependent transition to high-symmetry chiral structures in Ag-Cu, Ag-Co, Ag-Ni and Au-Ni nanoalloys, Nano Lett. 10 (2010) 4211.
[22] D. Bochicchio, R. Ferrando, Morphological instability of core-shell metallic nanoparticles, Phys. Rev. B 87 (2013) 165435.
[23] R. Ferrando, Symmetry breaking and morphological instabilities in core-shell metallic nanoparticles, J. Phys.: Condens. Matter 27 (2015) 013003.
[24] C. Langlois, Z.Y. Li, J. Yuan, D. Alloyeau, J. Nelayah, D. Bochicchio, R. Ferrando, C. Ricolleau, Transition from core-shell to Janus chemical configuration for bimetallic nanoparticles, Nanoscale 4 (2012) 3381.
[25] M.S. Cheng, D. Kumar, C.W. Yi, D.W. Goodman, The promotional effect of gold in catalysis by palladium-gold, Science 310 (2005) 291.
[26] A. Hugon, L. Delannoy, C. Louis, Selective hydrogenation of 1,3-butadiene in the presence of an excess of alkenes over supported bimetallic goldpalladium catalysts, J. Phys. Chem. C 114 (2010) 10823.
[27] F. Gao, Y. Wang, D.W. Goodman, Reaction kinetics and polarization-modulation infrared reflection absorption spectroscopy (PM-IRAS) investigation of CO oxidation over supported PdAu alloy catalysts, J. Phys. Chem. C 114 (2010) 4036.
[28] H. Zhang, T. Watanabe, M. Okumura, M. Haruta, N. Toshima, Catalytically highly active top gold atom on palladium nanocluster, Nature Materials 11 (2012) 49.
[29] F. Maroun, F. Ozanam, O.M. Magnussen, R.J. Behm, The role of atomic ensembles in the reactivity of bimetallic electrocatalysts, Science 293 (2001) 1811.
[30] C. Kittel, Introduction to solid state physics, 8th edition., Wiley, New York, 2005, p. 50.
[31] G. Rossi, A. Rapallo, C. Mottet, A. Fortunelli, F. Baletto, R. Ferrando, Magic polyicosahedral core-shell clusters, Phys. Rev. Lett. 93 (2004) 105503.
[32] F. Lequien, J. Creuze, F. Berthier, B. Legrand, Superficial segregation in nanoparticles: from facets to infinite surfaces, J. Chem. Phys. 125 (2006) 094707.
[33] J.P.K. Doye, M.A. Miller, D.J. Wales, The double-funnel energy landscape of the 38-atom Lennard-Jones cluster, J. Chem. Phys. 110 (1999) 6896.
[34] F. Pittaway, L.O. Paz-Borbo, R.L. Johnston, H. Arslan, R. Ferrando, C. Mottet, G. Barcaro, A. Fortunelli, Theoretical studies of palladium-gold nanoclusters: Pd-Au clusters with up to 50 atoms, J. Phys. Chem. C 113 (2009) 9141.
[35] G. Tréglia, B. Legrand, F. Ducastelle, A. Saùl, C. Gallis, I. Meunier, C. Mottet, A. Senhaji, Alloy surfaces: segregation, reconstruction and phase transitions, Comput. Mater. Sci. 15 (1999) 196.
[36] H. Okamoto, T.B. Massalski, in: T.B. Massalski (Ed.), Binary Alloy Phase Diagrams, second ed., vol. 1, ASM International, Materials Park, Ohio, 1990, p. 409.